Journal of Engineering Sciences

Vol 11, Issue 10,OCT /2020

ISSN NO:0377-9254

CONTROL OF A THREE-PHASE HYBRID CONVERTER FOR A PV CHARGING STATION USING PSO

[1]PAKA KEERTHI (M.TECH) ,[2]M.KRISHNA M.TECH (Assistant Professor)

ST. PETER'S ENGINEERING COLLEGE AND TECHNOLOGY, JNTU H, TELANGANA,

keerthi.paka243@gmail.com , krishnam@stpetershyd.com ,

ABSTRACT

Hybrid boost converter (HBC) has been proposed to replace a dc/dc boost converter and a dc/ac converter to reduce conversion stages and switching loss. In this paper, control of a three-phase HBC in a PV charging station is designed and tested. This HBC interfaces a PV system, a dc system with a hybrid plugin electrical vehicles (HPEVs) and a three-phase ac grid. The control of the HBC is designed to realize maximum power point tracking (MPPT) for PV, dc bus voltage regulation, and ac voltage or reactive power regulation. A test bed with power electronics switching details is built in MATLAB/Sim Powersystems for validation. Simulation results demonstrate the feasibility of the designed control architecture. Finally, lab experimental testing is conducted to demonstrate HBC's control performance.The control strategies can be used based on the combination between the Particle Swarm Optimization (PSO) method and the Proportional Integral (PI) controller that strategies can be extract the maximum power from a PV system. The PI Controller is used to tracking the maximum power from the PV panel, at different atmospheric condition. The Solar PV power generation system is comprised several elements like solar panel, DC-DC converter, MPPT Control Strategies and load.The Simulation result from MATLAB/SIMULINK is presented to verify the performance of the converter.

Index Terms—Plug-in hybrid vehicle (PHEV), Vector Control, Grid-connected Photovoltaic (PV), Three-phase Hybrid Boost Converter, Maximum Power Point Tracking (MPPT), Charging Station.

I. INTRODUCTION

T HE environmental and economic advantages of PHEV lead to the increase in number of production and consumption [1]. The U.S. Department of Energy forecasts that over one million PHEVs will be sold in the U.S. during the next decade [2]. Research has been conducted on developing a charging station by integrating a three-phase ac grid with PHEVs [3]–[5]. The comparison of different PHEV chargers' topologies and techniques are reviewed in [1], [6]. However, a large-scale penetration of PHEVs may add more pressure on the grid during charging periods. Therefore, charging stations with PV as an additional power source become a feasible solution. For PV charging stations, [7] proposed an architecture and controllers. The charging management is developed in [8] by considering the grid's loading limit. For this type of systems, it requires controlling at least three different power electronic converters to charge PHEVs. Each converter needs an individual controller, which increases complexity and power losses of the system. Consequently, it is urgent to investigate multi-port converters to reduce the number of converting stages. The objective of the paper is to implement such a multi-port converter in a PV charging station for PHEVs and design the controller.a maximum power point tracking (MPPT) method that can effectively track the global optimum of multipeak curves.This method was based on particle swarm optimization (PSO). Te concept of linear decreases in weighting was added to improve the tracking performance of the maximum power point tracker. Simulation results were used to verify that this method could successfully track maximum power points in the output characteristic curves of photovoltaic modules with multipeak values. The results also established that the performance of the modifed PSO-based MPPT method was superior to that of conventional PSO methods.

II. **PV Module** :Solar PV Module Solar panel absorbs the the photon energy from the sun and converts it into electricity using the photovoltaic (PV) effect principle. Thin-film or silicon material are used in the manufacturing of of PV modules. This will provide approximately constant power at low cost and also it is pollution free. A general PV cell produces maximum of 3 watts with nearly 1/2V dc. Number of PV cells connected in series or parallel to make a PV module.

1. SOLAR CELL CHARACTERISTICS The solar cell is mainly made of PV wafers, converts the light energy of solar irradiation into voltage and current directly for load, and conducts electricity without electrolytic effect. The electric energy is obtained from the PN interface of semiconductor directly; therefore, the solar cell is also known as PV cell .The equivalent circuit of solar cell as shown in Figure1

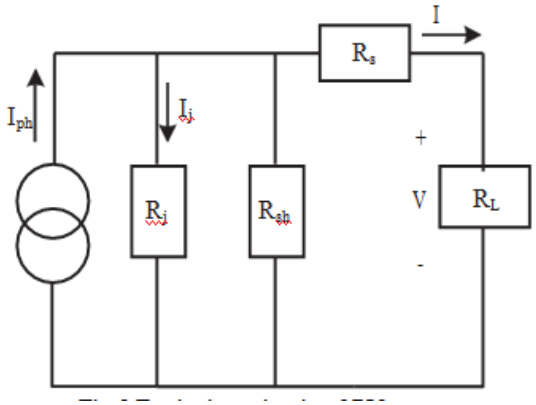

Fig1. Equivalent circuit of PV array

The current source Iph represents the cell photovoltaic current, Rj is used to represent the nonlinear resistance of the p-n junction, Rsh and Rs are used to represent the intrinsic shunt and series resistance respectively. Normally value of Rsh is very large and Rs is very small. Hence both of them can be neglected to simplify the analysis. PV cells are grouped in larger units to form PV modules. They are further interconnected in series-parallel combination to form PV arrays. The mathematical model used to simplify the PV array is represented by the equation

$$I = n_p I_{ph} - n_p I_{rs}\left[e^{\left(\frac{q}{kTA}\cdot\frac{V}{n_s}\right)} - 1\right]$$

Where I is the PV array output current, V is the PV array output voltage, ns is the number of series cells, np is the number of parallel cells, q is the charge of an electron, k is the Boltzman constant, A is the p-n junction ideality factor, T is the cell temperature, and Irs is the cell reverse saturation current. The factor A decides the deviation of solar cell from the ideal p-n junction characteristics. Its value ranges from one to five. The photo current Iph depends on the solar irradiance and cell temperature as below

$$I_{ph} = [I_{scr} + K_i(T - T_r)]\frac{S}{100}$$

Where Iscr is the cell short circuit current at reference temperature and radiation, Ki is the short circuit current temperature coefficient and S is the solar irradiance in mW/cm2. The Simulink model of PV array is shown in Fig. 4. The model includes three subsystems. One subsystem to model PV module and two more subsystems to model Iph and Irs.

III. THREE-PHASE HBC-BASED PV CHARGING STATION TOPOLOGY AND OPERATION

A three-phase HBC uses the same amount of switches as a two-level voltage source converter (VSC). However, the HBC can realize both dc/dc conversion and dc/ac conversion. As a comparison, Fig. 1 shows the conventional PV charging station where a dc/dc boost converter and a three-phase VSC are used to integrate the PV system, the PHEVs and the ac grid. A three-phase HBC replaces the two converters: the dc/dc boost converter and the dc/ac three-phase VSC to decrease the energy conversion stages and the power losses of the PV charging station. Fig. 2 shows the HBC-based PV charging station's topology. The main components of the configuration of the PV charging station consist of PV array, three-phase bidirectional HBC, ac grid, off-board dc/dc converter, and PHEV's batteries.

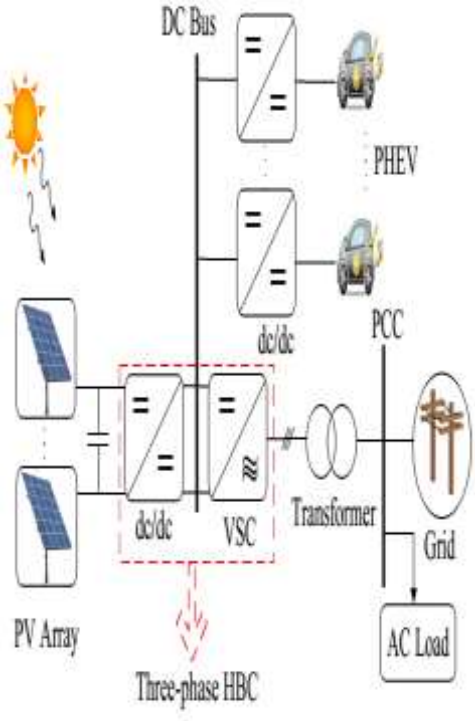

Fig. 2. Architecture configurations of a PV charging station. The conventional topology

includes a dc/dc converter and a dc/ac VSC. These two converters will be replaced by a three-phase HBC.

In order to design the control of a PV charging station, it is essential to understand the operation of a three-phase HBC. Detailed operation of an HBC can be found in [10], [11], [16]. Here a brief description is given.

The system is composed of a PV array, a dc system, a three-phase ac system, and the interfacing three-phase HBC as shown in Fig. 2. The PV side includes a large inductance to achieve continuous condition and capacitance to decrease the voltage ripple. The dc side includes a diode, a dc bus for PHEV connection, a dc capacitor to eliminate the output current ripples, an off-board unidirectional isolated dc/dc converter, and PHEV batteries. The ac system includes a three-phase LC filter, a step-up transformer, and the point of common coupling (PCC) bus that connects the PV station to the main grid.

The PV array is composed of connecting series cells and parallel strings. Each PV cell has specific characteristics depending on the type and designing criteria. PV models depend mainly on Shockley diode equation [17], [18]. PV can be modeled as a photon-generated current source in parallel with a two-diode system and a shunt resistor, R_{sh}, as well as in series with a series resistor, Rs. The mathematical equations of two-diode PV cell are given in [17]. HBC-based PV charging station has the capability to operate at medium and high power ratings of such PV power plants since a single IGBT-based VSC has the capability to operate at high voltage rating (e.g., voltage limitation up to1200 V [19]).] Traditional dc/dc boost converter is operated on two modes which are “on” and “off” states. Conventional VSC is operated on “active” and “zero” modes where the output ac power can have a value or zero. The three-phase HBC integrates the operational phases of a VSC and a dc/dc converter into three main modes. The main three intervals include a shoot-through (ST) mode, an active mode (A), and a zero mode (Z).

Some assumptions are considered to better illustrate the steady-state operation of the three-phase HBC. First, the system is assumed to be lossless where the damping elements equal zero. Second, the voltage drop on the diode is very small so it can be ignored. Next, the operational mode of the three-phase HBC is operated as an inverter where the power flows from the PV into the grid. It is recognized that the three-phase HBC can be operated at converter or inverter based on the direction of power flow. Finally, the diode current is continuous during the active phase. The steady-state relations between the PV, the dc side and the ac side are given as follows.

$$V_{dc} = \frac{V_{pv}}{1 - D_{st}}, \quad \hat{V}_{ac} = M_i \frac{V_{dc}}{2} \tag{1}$$

$$V_{LL} = M_i \frac{\sqrt{3}}{\sqrt{2}} \frac{V_{dc}}{2} = 0.612 \frac{M_i}{1 - D_{st}} V_{pv} \tag{2}$$

where M_i and D_{st} are the ac voltage per-phase modulation index and duty cycle of the shoot-through period, V_{dc}, V^ ac, and V_{LL} are the peak dc voltage, peak per-phase ac voltage, the RMS value of the line-to-line output ac voltage, respectively. It can be concluded from (2) that the dc output depends on only D_{st} while ac output depends on both D_{st} and Mi. In order to achieve continuous control of modified PWM, the controlling signals have to achieve this condition:

$$M_i + D_{st} < 1 \tag{3}$$

\A. Modified PWM

It is mentioned in Section II that the three-phase HBC is operated at three main intervals which are integrated between boost converter and VSC’s phases. Conventional sinusoidal

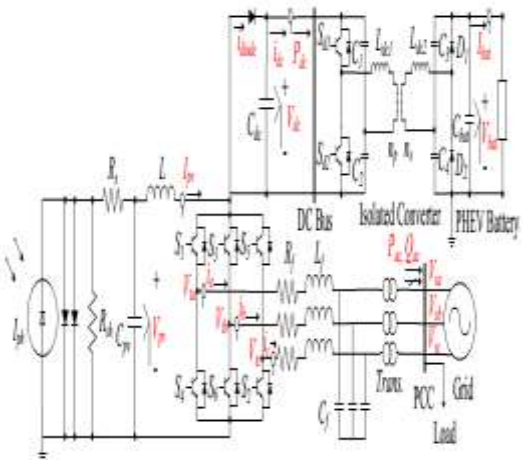

Fig. 3. Topology of the three-phase HBC-based PV charging station.

PWM and dc PWM are not appropriate to operate the switching states of three-phase HBC. Instead of separately controlling the dc and ac outputs using the switches of three-phase HBC,

a modified PWM is applied to control two outputs at the same time as shown in Fig. 3. It is recommended to insert the shoot-through phase within the zero mode where the output ac power equals zero in this phase [20]. During the shoot-through period, one leg of the two switchings, e.g., S1 and S4 are both on. This leads to PV side current flowing into S_1, S_4 only. During the shoot-through period, the inductor L gets charged. At the zero mode, all upper-level switches S1, S3 and S5 are on while the lower-level switches S4, S6 and S2 are off. At this mode, the PV side current all flows to the dc side battery systems while the current to the ac system is zero. Finally, during the active mode, current will flow into the ac system.

The behavior of the open-loop control scheme for switching states of the three-phase HBC is shown in Fig. 3 when the reference for the phase voltages are related as $V_a > V_b > V_c$. The shoot-through operation occurs when the positive signal V_{st} is lower than carrier signal (phase C is shoot through with S5 and S2) and when the negative signal V_{st} is greater than the carrier signal (phase A is shoot-through with S1 and S4 on).Shoot through happens at the phases with the highest voltage or lowest voltage. In Fig. 3, phase A and Phase C are the phases with shoot-through periods. Modified PWM regulates the switching states by controlling five signals which are three-phase ac signals V_a, V_b, V_c, and dc signals V_{st} ($V_{st} = 1 - D_{st}$), and $-V_{st}$. The ac controlling signals V_a, V_b, and V c are controlled by modulation index Mi as well as phase angles while the dc signals $+V_{st}$, and $-V_{st}$ are regulated by duty ratio D_{st}. The advantage of using modified PWM is that both dc and ac outputs can be adjusted.

IV. CONTROL OF PV CHARGING STATION

This section provides a detailed explanation on the framework and controller of the HBC-based PV charging station. From the steady-state relationship in (2), three-phase HBC utilizes D_{st} to boost the PV voltage while the modulation index Mi regulates the ac voltage V_t's magnitude. In addition, the angle of the three-phase ac voltage V_t can be adjusted to achieve active power and reactive power regulation. When the ac voltage is balanced and the ac system is symmetrical, the

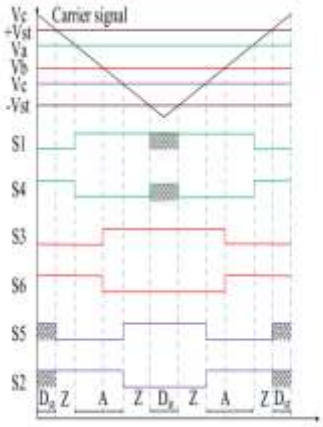

Fig. 4. A modified PWM for the three-phase-HBC. Shoot-through occurs when both switches are closed. ST, A, and Z are shoot-through, active, and zero periods, respectively.

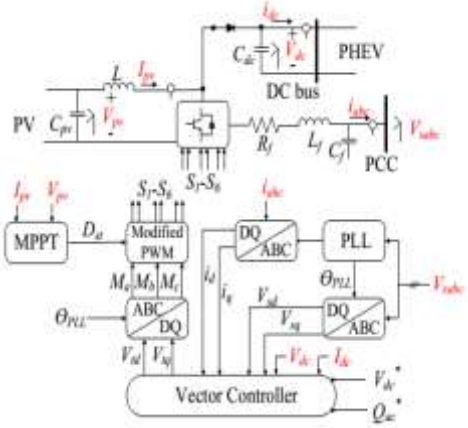

Fig. 5 Control blocks of the HBC-based PV charging station.

total three-phase instantaneous power is constant at steady state. Thus, average power of the ac side equals to the net power at the dc side ($P_{ac} = P_{pv} - P_{dc}$).

Three main control blocks are used to control the three phase HBC: MPPT, phase-locked loop (PLL) and vector control as shown in Fig. 4. Each block will be described by a subsection. The charging algorithm of the off-board isolated dc/dc converter will also be addressed in this section.

V. **particle swarm optimization**

In PSO, each single solution is a "bird" in the search space. We call it "particle". All of particles have fitness values, which are evaluated by the fitness function to be optimized, and have velocities, which direct the flying of the particles. The particles fly through the problem space by following the current optimum particles. When a particle takes part of the population as its topological neighbors, the best

value is a local best and is called p-best. Figure 6 shows the flowchart of Particle Swarm Optimization. In the particle swarm optimization algorithm, particle swarm consists of "n" particles, and the position of each particle stands for the potential solution in D-dimensional space. The particles change its condition according to the following three principles:

(1)To keep its inertia
(2) To change the condition according to its most optimist position
(3) To change the condition according to the swarm's most optimist position
The general flow chart of PSO can be described as follows:

PSO is a computational intelligence method that optimizes a problem by emulating a flock searching over candidate solutions (information carried by the particles) through search space. This algorithm allows all the random particles to search for the optimum solution in the search space through iterative process. Each particle will earn their best experience while interacting with each other to share their knowledge. PSO is a faster convergence and less parameters to tune and easier searching in very large problem spaces.

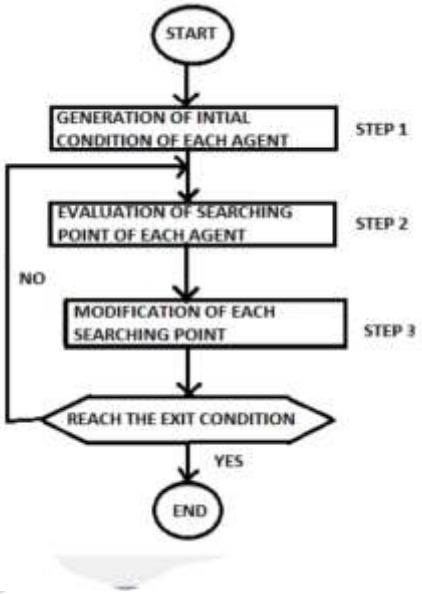

Flow Chart of PSO

Step 1: Generation of initial condition of each agent Initial searching points and velocities of each agent are usually generated randomly within the allowable range. The current searching point is set to pbest for each agent. The best evaluated value of pbest is set to gbest and the agent number with the best value is stored.

Step 2: Evaluation of searching point of each agent. The objective function value is calculated for each agent. If the value is better than the current pbest of the agent, the pbest value is replaced by the current value. If the best value of pbest is better than the current gbest, gbest is replaced by the best value and the agent number with the best value is stored.

Step 3: Modification of each searching point. The current searching point of each agent is changed.
Step 4: Checking the exit condition such as maximum number of iteration

The PSO Algorithm having following advantages such as,

(i) PSO is based on the intelligence. It can be applied into both scientific research and engineering use.
(ii) PSO have no overlapping and mutation calculation. The search can be carried out by the speed of the particle. During the development of several generations, only the most optimist particle can transmit information onto the other particles, and the speed of the researching is very fast.
(iii) The calculation in PSO is very simple. Compared with the other developing calculations, it occupies the bigger optimization ability and it can be completed easily.
(iv) PSO adopts the real number code, and it is decided directly by the solution. The number of the dimension is equal to the constant of the solution

The purpose of PSO

The usual aim of the particle swarm optimization (PSO) algorithm is to solve an unconstrained minimization problem: find x* such that f(x*)<=f(x) for all d-dimensional real vectors x. The objective function f: Rd -> R is called the fitness function.

History of PSO

PSO has been proposed by Eberhart and Kennedy in 1995, subsequently developed in thousands of scientific papers, and applied to many diverse problems, for instance neural networks training, data mining, signal processing, and optimal design of experiments.

Basic description of PSO

PSO is a swarm intelligence meta-heuristic inspired by the group behavior of animals, for example bird flocks or fish schools. Similarly to genetic algorithms (GAs), it is a population-

based method, that is, it represents the state of the algorithm by a population, which is iteratively modified until a termination criterion is satisfied. In PSO algorithms, the population P={p1,…,pn} of the feasible solutions is often called a swarm. The feasible solutions p1,…,pn are called particles. The PSO method views the set R d of feasible solutions as a "space" where the particles "move". For solving practical problems, the number of particles is usually chosen between 10 and 50

Swarm topology

Each particle i has its neighborhood Ni (a subset of P). The structure of the neighborhoods is called the swarm topology, which can be represented by a graph. Usual topologies are: fully connected topology and circle topology.

Characteristics of particle i at iteration t:

xi (t) … the position (a d-dimensional vector)

pi (t) … the "historically" best position

li (t) … the historicaly best position of the neighboring particles; for the fully connected topology it is the historically best known position of the entire swarm

vi (t) … the speed; it is the step size between xi (t) and xi (t+1) At the beginning of the algorithm, the particle positions are randomly initialized, and the velocities are set to 0, or to small random values.

Parameters of the algorithm:

w (t) … inertia weight; a damping factor, usually decreasing from around 0.9 to around 0.4 during the computation

φ1, φ2 … acceleration coefficients; usually between 0 and 4.

Update of the speed and the positions of the particles

Many versions of the particle speed update exist, for example:

vi (t+1) =w (t) vi (t)+ φ1u1(pi (t) -xi (t))+ φ2u2(li (t) -xi (t)).

The symbols u1 and u2 represent random variables with the U(0,1) distribution. The first part of the velocity formula is called "inertia", the second one "the cognitive (personal) component", the third one is "the social (neighborhood) component". Position of particle i changes according to xi (t+1) = xi (t) +vi (t+1) .

Stopping rule The algorithm is terminated after a given number of iterations, or once the fitness values of the particles (or the particles themselves) are close enough in some sense.

PSO variants There is a plethora of different versions of PSOs, which usually modify the formula for the change of velocity (e.g., instead of u1 and u2 they use diagonal matrices U1 and U2, in other variants they use no inertia, but enforce an upper limit on the particle speed, there is the so-called "fully informed" PSO, and there is also a popular modification using a "constriction coefficient"). There exist versions of the PSO for constrained optimization, for discrete optimization, and for multi-objective optimization.

The PSO calculation process is as follows.
(1) Set the number of particles, the maximum number of iterations, the weight, and the learning factors.
(2) Initialize the particle swarm and randomly assign positions and velocities for each particle.
(3) Substitute the initial positions into the objective function to assess the fitness values for each particle.
(4) Compare the fitness values and the individual best memory positions Pbest of each particle to select better positions and update Pbest.

(5) compare Pbest and the swarm best memory value Gbest If Pbest is superior to Gbest update Gbest.

(6) Use the core PSO formulas to update particle velocities and positions. These formulas are shown as follows:

$$V_i^{j+1} = W \times V_i^j + C_1 \times \text{rand1}(\bullet) \times \left(P_{\text{best}} - P_i^j\right) + C_2 \times \text{rand2}(\bullet) \times \left(G_{\text{best}} - P_i^j\right),$$

$$P_i^{j+1} = V_i^{j+1} + P_i^j.$$

(7) Stop tracking if the stop conditions are met. Otherwise, rerun Steps 4 through 6. To stop conditions are either locating the global optimum or reaching the maximum number of iterations.

The search efficiency and success rate of PSO are determined primarily by the values assigned for the weights and the learning factors . When the weight is too high, the particle search might lack accuracy because the movement step sizes are too large. However, if the weight is low, particle movement becomes slow, and the local optimum trap might be unavoidable when facing multi-peak values. Thus, weighting is typically based on the objective function.

Conventional PSO is fast and accurate when searching for the output characteristic curves of PV module arrays with single peak values. However, when some modules are shaded, weights in conventional PSO must be readjusted appropriately based on various multipeak curve characteristics. If this is not performed, excessively high or low weights result in tracking failure. Thus, conventional PSO-based MPPT must be modified when some of the modules in a photovoltaic module array are shaded. To solve these problems, linear decreases in line with
increasing iteration numbers were adopted in this study for the weighting of the PSO kernel formulas. To modified weighting formula is as follows:

$$W = (W_{\max} - W_{\min}) \times \frac{(n-j)}{n} + W_{\min},$$

The physical meaning of this modified weighting formula is that greater step sizes are used to increase the particle search velocity during the initial search because the distance to the global optimum is relatively large. This prevents an excessively small step size from making local optimum traps unavoidable. However,

$$P_{\text{best}_i} = \begin{cases} P_{\text{best}_i}, & P_{\text{best}_i} > 0, \\ 0, & P_{\text{best}_i} \le 0. \end{cases}$$

$$P_{\text{best}_i} = P_i^{j+1}.$$

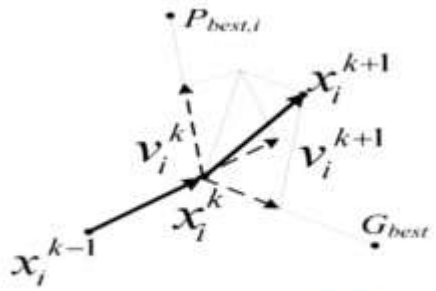

Fig. Movement of a PSO particle

The movement of particles impact by two variables; the Pbest that used to store the best position of each particle as an individual best position, and the Gbest that found by comparing individual positions of the particle swarm and store it as best position of the swarm. The particle swarm uses this process to move towards the best position and continuously it revise its direction and velocity, by this way, each particle quickly converge to an optimal or close to a global optimum.

VI. Simulation results :

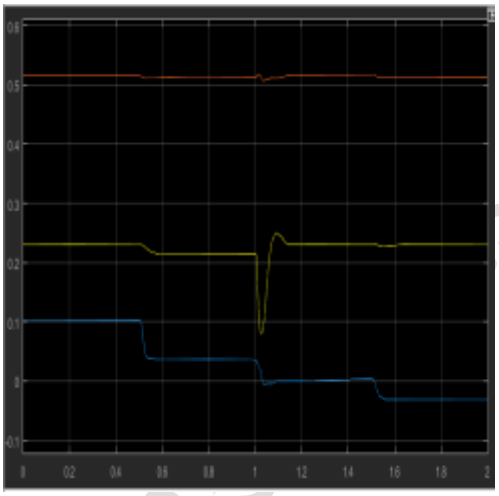

Fig. 6. Dst, Md and Mq

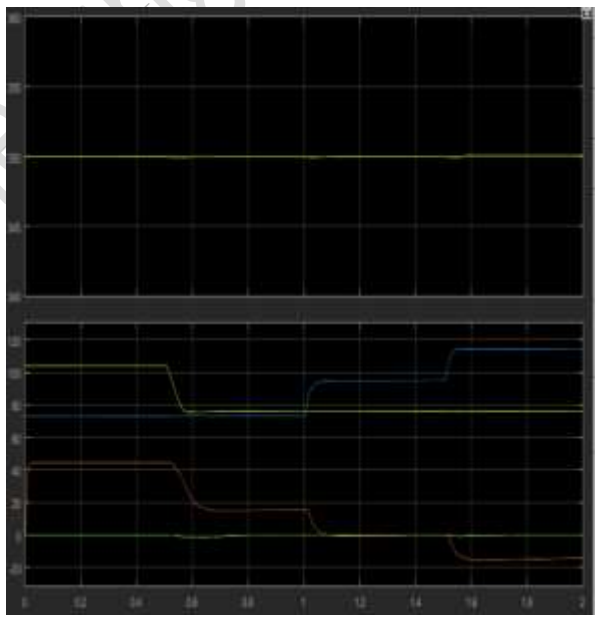

Fig. 7. Power management of PV charging station.

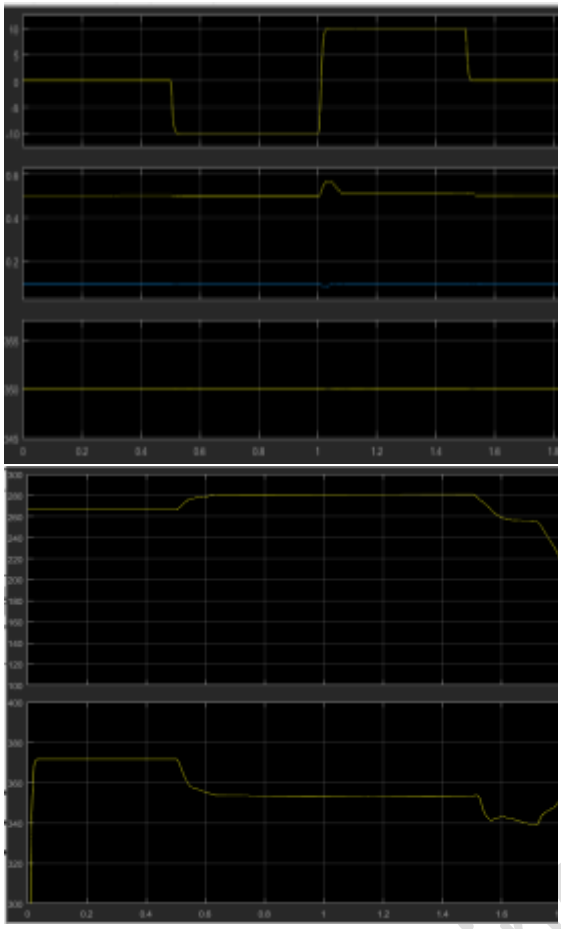

Fig. 8. Performance of the dc voltage control in the vector control. The solid lines represent the system responses when the dc voltage control is enabled. The dashed lines represent the system responses when the dc voltage control is disabled.

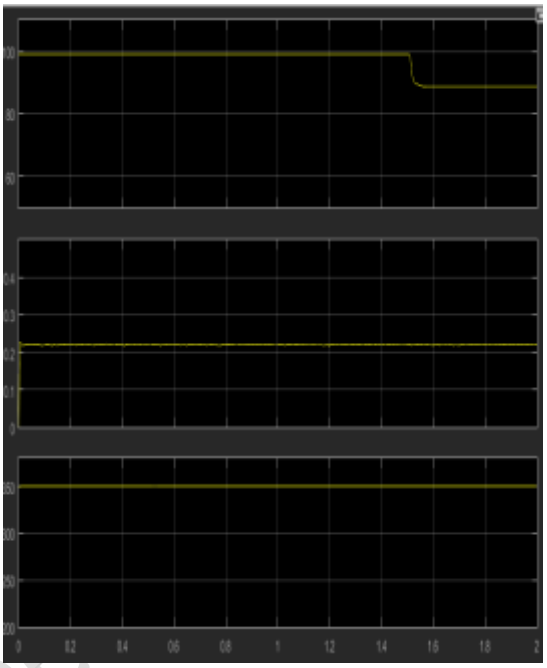

Fig.9. Performance of a modified IC-PI MPPT algorithm when solar irradiance variation is applied.

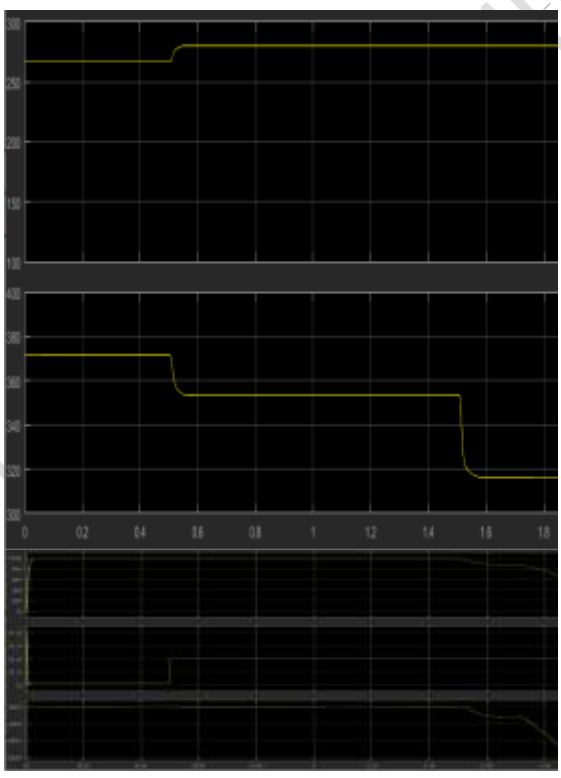

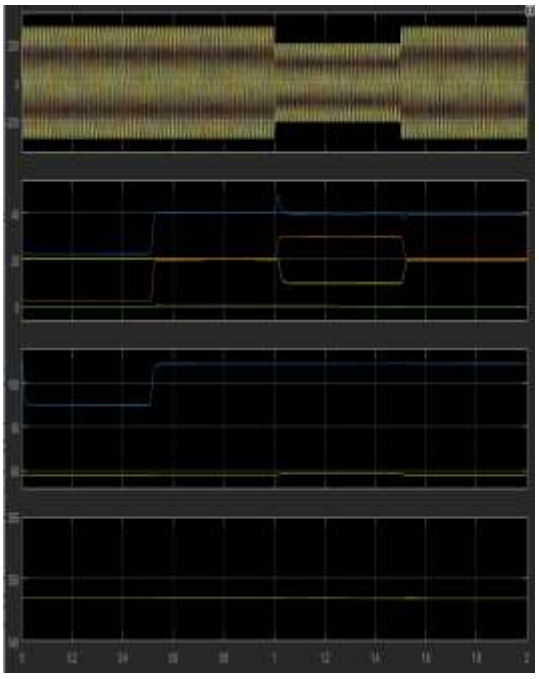

Fig. 10. System performance under 70% grid's voltage drop.

VII. CONCLUSION

Control of three-phase HBC in a PV charging station is proposed in this paper. The three-phase HBC can save switching loss by integration a dc/dc booster and a dc/ac converter converter into a single converter structure. A new control for the three-phase HBC is designed to achieve MPPT, dc voltage regulation and reactive power tracking. The MPPT control utilizes modified incremental conductance-PI based MPPT method. The dc voltage regulation and reactive power tracking are realized using vector control. Five case studies are conducted in computer simulation to demonstrate the performance of MPPT, dc voltage regulator, reactive power tracking and overall power management of the PV charging station. Experimental results verify the operation of the PHEV charging station using HBC topology. The simulation and experimental results demonstrate the effectiveness and robustness of the proposed control for PV charging station to maintain continuous dc power supply using both PV power and ac grid power.The primary feature of this method is the linear decreases used to adjust weighting, in contrast to the fixed weights adopted by conventional PSO. Te modified PSO method was applied to maximum power tracking in photovoltaic module arrays, successfully solving the inability to track true MPPs because of partial module shading in photovoltaic module arrays. The tracking success rate reached 100% for the modified method, and the tracking speed was superior to that of conventional PSO. This could reduce energy loss during the MPPT process, thereby substantially enhancing the power generation efficiency of photovoltaic power generation systems.

VIII. REFERENCES

[1] M. Ehsani, Y. Gao, and A. Emadi, Modern electric, hybrid electric, and fuel cell vehicles: fundamentals, theory, and design. CRC press, 2009.

[2] K. Sikes, T. Gross, Z. Lin, J. Sullivan, T. Cleary, and J. Ward, “Plugin hybrid electric vehicle market introduction study: final report,” Oak Ridge National Laboratory (ORNL), Tech. Rep., 2010.

[3] A. Khaligh and S. Dusmez, “Comprehensive topological analysis of conductive and inductive charging solutions for plug-in electric vehicles,” IEEE Transactions on Vehicular Technology, vol. 61, no. 8, pp. 3475– 3489, 2012.

[4] T. Anegawa, “Development of quick charging system for electric vehicle,” Tokyo Electric Power Company, 2010.

[5] F. Musavi, M. Edington, W. Eberle, and W. G. Dunford, “Evaluation and efficiency comparison of front end ac-dc plug-in hybrid charger topologies,” IEEE Transactions on Smart grid, vol. 3, no. 1, pp. 413– 421, 2012.

[6] M. Yilmaz and P. T. Krein, “Review of battery charger topologies, charging power levels, and infrastructure for plug-in electric and hybrid vehicles,” IEEE Transactions on Power Electronics, vol. 28, no. 5, pp. 2151–2169, May 2013.

[7] G. Gamboa, C. Hamilton, R. Kerley, S. Elmes, A. Arias, J. Shen, and I. Batarseh, “Control strategy of a multi-port, grid connected, direct-dc pv charging station for plug-in electric vehicles,” in Energy Conversion Congress and Exposition (ECCE), 2010 IEEE. IEEE, 2010, pp. 1173– 1177.

[8] P. Goli and W. Shireen, “Pv integrated smart charging of phevs based on dc link voltage sensing,” IEEE Transactions on Smart Grid, vol. 5, no. 3, pp. 1421–1428, 2014.

[9] S. Mishra, R. Adda, and A. Joshi, “Inverse watkins–johnson topologybased inverter,” IEEE Transactions on Power Electronics, vol. 27, no. 3, pp. 1066–1070, 2012.

[10] O. Ray and S. Mishra, “Boost-derived hybrid converter with simultaneous dc and ac outputs,” IEEE Transactions on Industry Applications, vol. 50, no. 2, pp. 1082–1093, March 2014.

[11] O. Ray, V. Dharmarajan, S. Mishra, R. Adda, and P. Enjeti, “Analysis and pwm control of three-phase boost-derived hybrid converter,” in 2014 IEEE Energy Conversion Congress and Exposition (ECCE), Sept 2014, pp. 402–408.

[12] O. Ray and S. Mishra, “Integrated hybrid output converter as power router for renewable-based nanogrids,” in Industrial Electronics Society, IECON 2015 - 41st Annual Conference of the IEEE, Nov 2015, pp. 001 645–001 650.

[13] M. A. Elgendy, B. Zahawi, and D. J. Atkinson, “Assessment of perturb and observe mppt algorithm implementation techniques for pv pumping applications,” IEEE transactions on

sustainable energy, vol. 3, no. 1, pp. 21–33, 2012.

[14] J. Khazaei, Z. Miao, L. Piyasinghe, and L. Fan, "Real-time digital simulation-based modeling of a single-phase single-stage pv system," Electric Power Systems Research, vol. 123, pp. 85–91, 2015.

[15] M. Tabari and A. Yazdani, "Stability of a dc distribution system for power system integration of plug-in hybrid electric vehicles," IEEE Transactions on Smart Grid, vol. 5, no. 5, pp. 2564–2573, 2014. [16] O. Ray and S. Mishra, "Integrated hybrid output converter as power router for renewable-based nanogrids," in Industrial Electronics Society, IECON 2015-41st Annual Conference of the IEEE. IEEE, 2015, pp. 001 645–001 650.

[17] U. Eicker, Solar technologies for buildings. John Wiley & Sons, 2006.

[18] N. Femia, G. Petrone, G. Spagnuolo, and M. Vitelli, Power electronics and control techniques for maximum energy harvesting in photovoltaic systems. CRC press, 2012.